Proceedings of the 2007 American Control Conference
Marriott Marquis Hotel at Times Square
New York City, USA, July 11-13, 2007

Adaptive Disturbance Rejection for Flow in a Duct with Time-Varying Upstream Velocity

Mario A. Santillo, Jesse B. Hoagg, Dennis S. Bernstein, Kenneth Powell

Department of Aerospace Engineering,
The University of Michigan,
Ann Arbor, MI 48109-2140
{santillo, jhoagg, dsbaero, powell}@umich.edu

Abstract— **In this paper we demonstrate adaptive flow control for an incompressible viscous fluid through a two-dimensional channel without using an analytical model. An adaptive disturbance rejection algorithm is implemented within a CFD simulation to reduce the effects of an unknown time-varying inlet velocity disturbance on the performance variable, which is the longitudinal velocity component of the flow at a downstream location. The algorithm requires minimal knowledge of the system, specifically, the numerator coefficients of the transfer functions from the control inputs to the performance variable. System identification, based on CFD simulation prior to disturbance rejection, is used to identify the required parameters.**

I. Introduction

Active flow control has attracted increasing attention over the past several years. Applications include improving the aerodynamics of aerospace vehicles, such as reducing drag and increasing lift on a wing, suppressing vortex shedding around bluff bodies, altering flow characteristics in compressors by relaminarizing flow to reduce power consumption, minimizing drag penalties in mixing processes such as the air-fuel mixture in combustion engines, and reducing noise emissions. The potential benefits of active flow control are only beginning to be realized. An overview of flow control is given by [1].

Among the standard control techniques that have been applied to active flow control are PI and LQG controllers [2]–[4] based on models of the linearized Navier-Stokes equation, obtained by a Galerkin procedure. LQG/LTR control of the streamfunction formulation of the Navier-Stokes equation is used in [5], [6] to achieve drag reduction below the laminar level. An LQG controller based on a reduced-order model obtained from a finite element code is used in [7]. In addition, a nonlinear control law is developed in [8], where a Galerkin method is used to derive a reduced-order model of the two-dimensional Navier-Stokes equation. Alternative methods presented in [9]–[11] include PDE-based control, robust control, and predictive control with direct numerical simulation (DNS). Dynamic stall and flow separation control by periodic excitation are discussed in [12]–[14].

Additional techniques include a MATLAB-FEATFLOW DNS coupling in [15] to control the recirculation bubble behind a backward-facing step. In [16] a CFD simulation, along with NARMAX identification and linear feedback control, is used to control flow separation using synthetic jets. Traditional Galerkin methods are used in [17], [18] to regulate the flow behind a cylinder wake. A robust $\mathcal{H}_\infty$ controller is used in [19] to control the reattachment length downstream of a backward-facing step.

An alternative to pure model-based control methods is to use adaptive control. In [20], the ARMARKOV disturbance rejection algorithm is used for a weapons-bay suppression system. Adaptive control of flow-induced cavity oscillations is considered in [21]. Robust and adaptive methods are compared in [22] for controlling the recirculation length behind a backward-facing step, the lift of a generic high-lift configuration, and pressure recovery in a diffusor flow. Adaptive extremum-seeking controllers are employed in [23]–[25] to regulate the flow behind a backward-facing step, minimize the drag of a bluff body, and reduce noise emissions in turbomachinery. In [26], the ARMARKOV algorithm is used in a two-dimensional channel CFD simulation to reduce the effects of an unknown transverse velocity disturbance on a downstream performance variable, and in [27], the algorithm is used to modify the steady-state flow field in a 2D channel.

The goal of this paper is to apply ARMARKOV disturbance rejection to a CFD simulation of 2D channel Poiseuille (viscous) flow with a time-varying upstream velocity disturbance. We thus consider a two-dimensional channel with velocity sensors y and z and control jets u_1 and u_2, where the goal is to reduce the effects of an unknown time-varying inlet velocity disturbance using the control jets. The disturbance $w(t)$ is superimposed on the nominal channel inlet velocity V_0. This problem arrangement is motivated by applications where it is desired to maintain nominal flow conditions despite upstream variations.

Flow control using the ARMARKOV adaptive algorithm differs from model-based control methods since a detailed model of the flow is not required. Instead, a CFD simulation is used to generate input/output data from which the essential model parameters are extracted. The identification is performed by perturbing the flow with band-limited white noise applied at the control jets. The numerator coefficients of an ARMARKOV model are then identified off-line. Adaptive flow control is achieved by a compensator whose parameter

Supported by the Air Force Office of Scientific Research under a National Defense Science and Engineering Graduate Fellowship.

matrix is updated on-line by a gradient algorithm. An alternative method for identifying fluid-dynamic systems is given by [28].

To apply this technique, we first use a CFD simulation coupled with system identification to obtain the numerator coefficients of the transfer functions from the control inputs to the performance variable. Alternatively, measurements obtained from the physical system can be used for identification assuming that external disturbance levels are manageable compared to the identification input. Adaptive flow control using the ARMARKOV algorithm can then be implemented in real time on the physical system.

II. Problem Statement and Description

Consider the 2D channel geometry shown in Figure 1. Let $u_1(t) \in \mathbb{R}$ be the control signal applied to the flow on the lower wall, $u_2(t) \in \mathbb{R}$ be the control signal applied to the flow on the upper wall, $y(t) \in \mathbb{R}$ the measurement variable, and $z(t) \in \mathbb{R}$ the performance variable. Here $y(t)$ and $z(t)$ are deviations from the nominal longitudinal velocity components of the flow at the sensor locations. The control signals $u_1(t)$ and $u_2(t)$ represent mass flow velocities normal to the channel walls into (or out of) the system. The goal is to reduce the effects of an unknown channel inlet velocity disturbance $w(t) \in \mathbb{R}$ using the control jets. The inlet disturbance is superimposed on the nominal channel inlet velocity $V_0 > 0$; the total velocity at the inlet is thus $V_\infty(t) = V_0 + w(t)$.

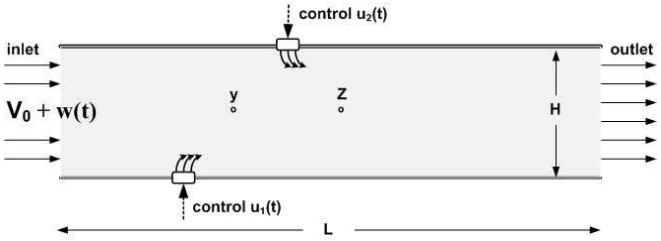

Fig. 1. 2D channel geometry for adaptive flow control.

The wall separation distance is $H = 0.25$ m, and the channel length is $L/H = 12$. Two suction/blowing jets, through orifices of width $0.2H$, are located in the walls of the channel, the first to apply control along the lower wall, located at $x_{u_1}/H = 3$ from the channel inlet on the lower wall, and the second to apply control along the upper wall, located at $x_{u_2}/H = 5$ from the channel inlet on the upper wall. Measurement and performance velocity sensors y and z are located in the center of the channel at $x_y/H = 4$ and $x_z/H = 6$, respectively, from the channel inlet.

For simulation, we take the nominal channel inlet velocity to be $V_0 = 0.02$ m/s and assume that the fluid is incompressible. Taking the fluid as air at standard temperature and pressure, dynamic viscosity $\mu = 1.7894 \times 10^{-5}$ kg/m-s, and wall separation distance as the characteristic length, the Reynolds number is $\mathrm{Re}_H = 350$.

III. CFD Simulation Setup

A 2D, segregated, unsteady, implicit, second-order solver is used for the CFD simulations. This configuration allows us to capture the effects of the fluid motion while staying well below transition to turbulence. The use of a small Reynolds number also allows us to assume that the fluid system is incompressible.

The CFD mesh is a rectangular grid with cell size 0.01 m $\times$ 0.005 m ($0.04H \times 0.02H$), resulting in 300 streamwise cells and 50 wall normal cells. The simulation step size is 0.01 s, which allows frequency domain analysis up to 50 Hz. The channel inlet and both control jets are defined as velocity inlets, while the channel outlet is a pressure outlet. The pressure drop across the outlet is set to be zero.

Figure 2 provides a software flow chart of the simulation process. The two-dimensional channel is simulated within the CFD software Fluent, a commercial computational fluid dynamics software package available from Fluent, Inc. [29]. Using the User Defined Functions (UDFs) within Fluent, C-program functions were written and connected to the CFD simulation.

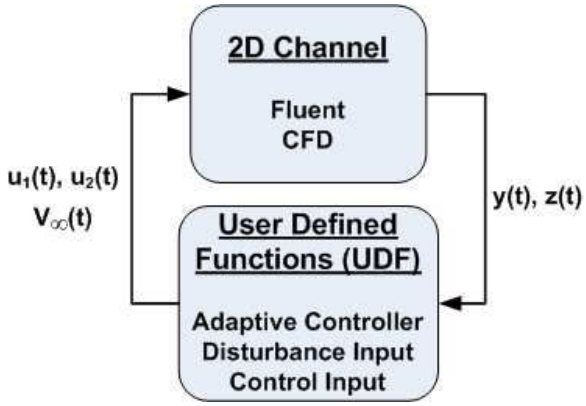

Fig. 2. Software flow chart for CFD-based adaptive flow control.

At every time step within the simulation, the boundary conditions at the channel inlet are set according to the output of the disturbance UDF. Also, the measurement and performance variables $y(t)$ and $z(t)$ are read directly into the adaptive control UDF. These sensor measurements, along with the data obtained from off-line system identification (completed before closed-loop CFD simulations, see Section V), are used to calculate the appropriate velocity values to apply at the control jets u_1 and u_2. The boundary conditions at the control jets are then updated directly from the control UDF. ASCII text files are used to transfer data to and from the simulation environment, which are subsequently used for post-processing the simulation results.

To facilitate the computation, the simulation is written to run in a parallel computing environment. In particular, the C-programming code requires parallel computing notation for data input/output by the computing cluster. Simulations are run on dual-processor nodes. The use of two processors is most efficient for our CFD mesh; beyond two processors,

the simulation times increase due to communication delays between the compute nodes.

IV. Adaptive Disturbance Rejection Algorithm Development

CFD-based adaptive flow control is based on the ARMARKOV disturbance rejection algorithm [30], [31] implemented within the CFD software Fluent. The ARMARKOV algorithm is applied to various experimental testbeds in [32]–[41] and is demonstrated on fluid dynamic systems in [26], [27].

To develop a rigorous framework for the ARMARKOV algorithm, logarithmic Lyapunov functions are shown in [42] to be useful in convergence proofs for discrete-time adaptive controllers. Logarithmic Lyapunov functions aid in proving Lyapunov stability in the discrete-time setting since the key technical lemma [43] does not guarantee Lyapunov stability. Logarithmic Lyapunov functions are used in [44] to prove Lyapunov stability for discrete-time model reference adaptive control when the normalized projection algorithm is used for parameter identification. A variation of the ARMARKOV algorithm with provable convergence properties for adaptive stabilization, command following, and disturbance rejection for minimum-phase discrete-time systems is presented in [45].

V. System Identification

To obtain the required controller parameters for the ARMARKOV model, a CFD simulation is used with band-limited white noise injected into undisturbed ($V_\infty(t) \equiv V_0, w(t) = 0$) laminar flow from the control jets. The input and performance velocity measurements are recorded at a sampling rate of 100 Hz.

We implement the time-domain ARMARKOV/Toeplitz system identification technique [32], [33] to extract the required controller parameters, specifically the numerator coefficients of the transfer functions from the control inputs to the performance variable. These coefficients are subsequently used by the adaptive controller during closed-loop simulations.

VI. Results

To test the adaptive disturbance rejection algorithm, a longitudinal velocity disturbance $w(t)$ is applied at the channel inlet, superimposed on the nominal channel inlet velocity of $V_0 = 0.02$ m/s, yielding the total channel inlet velocity $V_\infty(t) = V_0 + w(t)$. Three cases are considered. We first use a single-tone signal to disturb the nominal flow in the channel. Here, the disturbance $w(t)$ is a sine wave with constant frequency and constant amplitude applied to the channel inlet, in addition to the nominal channel inlet velocity V_0. Next, the disturbance signal is chosen to have two harmonic components. Finally, we use a filtered band-limited white noise signal to disturb the flow. In all cases, although the disturbance is created within the simulation, the controller has no knowledge of the disturbance. The nominal channel inlet velocity V_0 is used to nondimensionalize all velocities in the following results.

A. Single-tone Disturbance

For a single-tone disturbance, the amplitude of the disturbance signal $w(t)$ is chosen to be 50% of the nominal channel inlet velocity V_0. Figure 3 shows the deviation from nominal in the longitudinal velocity at the location of z for both the open-loop and closed-loop responses to a disturbance signal at 0.1 Hz. The adaptive disturbance rejection controller decreases the deviation in longitudinal velocity within a few seconds. Figure 4 shows the power spectral density of both the open-loop response and the closed-loop response. A reduction of about 100 dB in the closed-loop response is achieved at the disturbance frequency of 0.1 Hz. Due to the nonlinearity of the flow dynamics, multiple harmonics remain; however, the power at these frequencies is less than at the 0.1-Hz fundamental frequency. Note that the nondimensionalized longitudinal velocity at z is greater than 1; this is to be expected since the channel flow is fully developed at this location ($x_z/H = 6$).

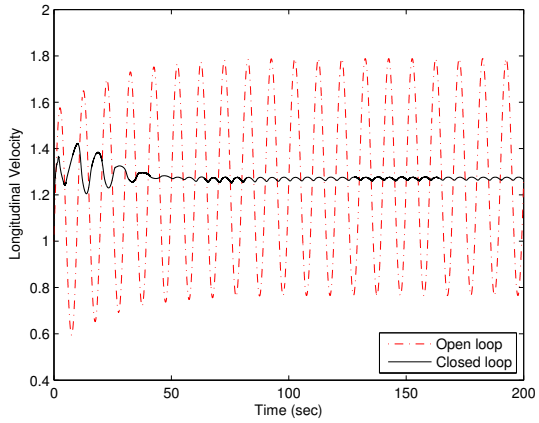

Fig. 3. Open-loop and closed-loop longitudinal performance velocity response for a single-tone 0.1-Hz disturbance.

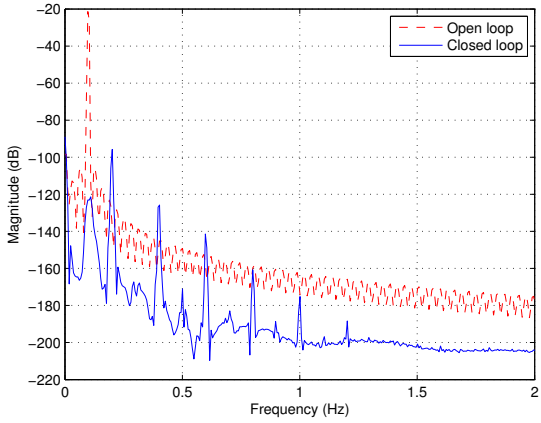

Fig. 4. Open-loop and closed-loop power spectrum for a single-tone 0.1-Hz disturbance.

The results shown in Figures 3 and 4 are obtained with a controller order of $n_c = 50$. For all simulations the

controller order is varied in increments of 5 between 25 and 50. Although a higher order controller generally improves disturbance rejection, the improvements are not significant above $n_c = 30$. No computational difficulties arise from increasing the controller order beyond $n_c = 25$.

In addition to varying the controller order, the effect of varying the disturbance frequency is also investigated. Figure 5 shows the the deviation from nominal in the longitudinal velocity at the location of z for both the open-loop and closed-loop responses to a disturbance signal at 0.2 Hz. The adaptive disturbance rejection controller decreases the perturbation in longitudinal velocity within a few seconds. Figure 6 shows the power spectral density of both the open-loop response and the closed-loop response. A reduction of about 120 dB in the closed-loop response is achieved at the disturbance frequency of 0.2 Hz. It is interesting to note that, in this case, the higher harmonics do not cause spillover (in the sense of [46]), as is the case with a 0.1-Hz disturbance.

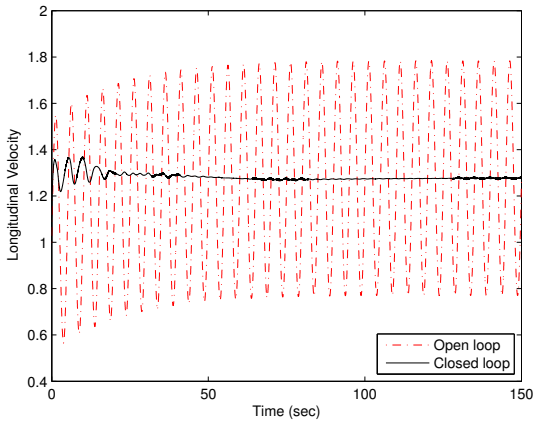

Fig. 5. Open-loop and closed-loop longitudinal performance velocity response for a single-tone 0.2-Hz disturbance.

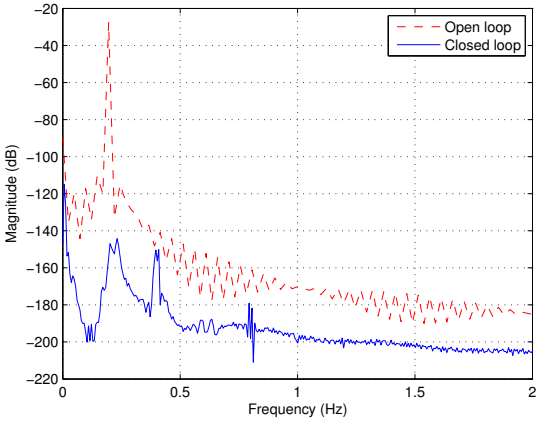

Fig. 6. Open-loop and closed-loop power spectrum for a single-tone 0.2-Hz disturbance.

B. Dual-tone Disturbance

Next, a dual-tone signal is used to disturb the nominal channel flow. The amplitude of the disturbance signal $w(t)$ is chosen to be 50% of the nominal channel inlet velocity V_0. Dual frequency disturbance rejection is simulated as in the single frequency case, with the only change being in the UDF used to drive the disturbance. Figure 7 shows both the open-loop and closed-loop responses to a disturbance containing 0.1-Hz and 0.15-Hz components. The controller is seen to reduce the deviation from nominal in the longitudinal velocity at the location of z in about 100 seconds. Figure 8 shows the power spectral density of the open-loop and closed-loop response to the dual-tone disturbance. A decrease of up to 50 dB in the closed-loop response is seen at both disturbance frequencies. The maximum control effort is approximately twice the nominal channel inlet velocity V_0, as shown in Figure 9.

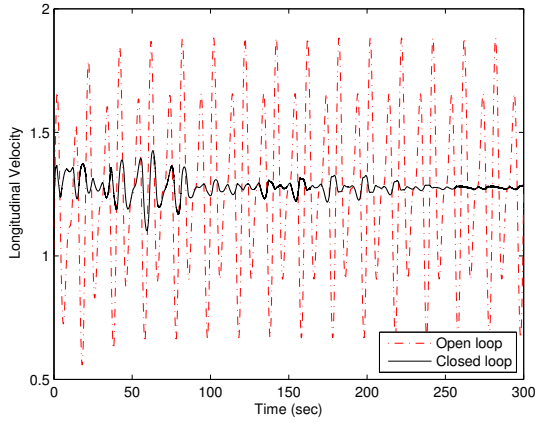

Fig. 7. Open-loop and closed-loop longitudinal performance velocity response for dual-tone 0.1-Hz and 0.15-Hz disturbance.

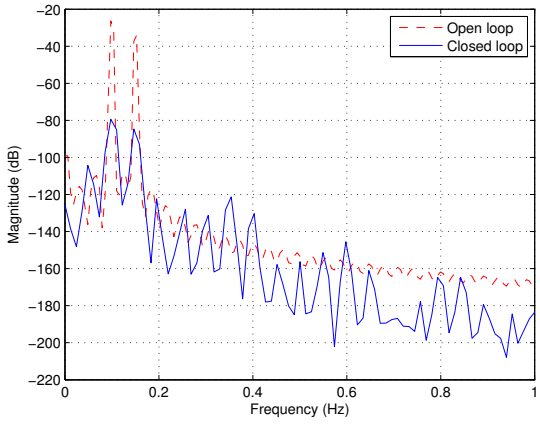

Fig. 8. Open-loop and closed-loop power spectrum for dual-tone 0.1-Hz and 0.15-Hz disturbance.

As with the single-tone case, the disturbance spectrum and the controller order are varied. Although most disturbance frequency pairs between 0.05 Hz and 1.0 Hz are rejected by

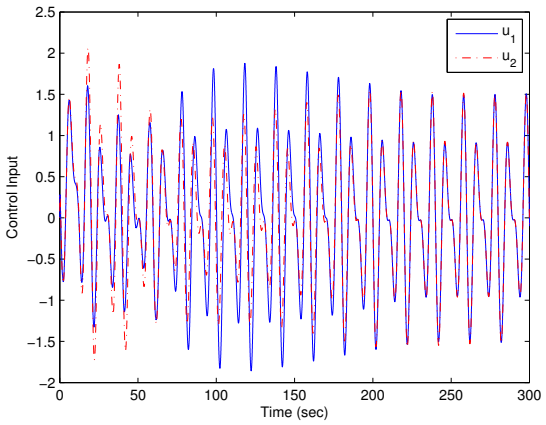

Fig. 9. Closed-loop control input velocity for dual-tone 0.1-Hz and 0.15-Hz disturbance.

the controller, there exist cases where disturbance rejection is not obtained. The nonlinear effect of the channel flow dynamics in some cases produces strong super and sub harmonics that are not removed by the controller. In these cases the magnitude of the closed-loop performance is less than the open-loop response but not to the extent shown in Figure 8.

Varying controller order for the dual-tone case is found to have both a positive and negative effect. In the case of a 0.05-Hz and 0.09-Hz dual-tone disturbance, as the controller order is increased in increments of 5 above $n_c = 30$, the rejection of the fundamental frequencies stays nearly the same, however, spillover occurs at both super and sub harmonics. This spillover leads to an overall larger magnitude steady-state response of the longitudinal performance variable z. In most simulations a controller order is found that reduces the fundamental frequencies with reasonable attenuation of both super and sub harmonics.

C. White Noise Disturbance

The third case involves band-limited white noise as the disturbance signal. The band-limited white noise disturbance is generated prior to the CFD simulation using Simulink's Band-Limited White Noise block with noise power 0.00001 W/Hz and then passing the data through a second-order filter with $\zeta = 0.05$ and $\omega_n = 16$ rad/sec. The filtered data are limited to a frequency band of approximately 1 Hz to 5 Hz, with zero mean and standard deviation $\sigma = 0.0015$ m/s. The disturbance data are then saved to an ASCII text file; the text file is read during the simulation and applied at the channel inlet as $w(t)$, superimposed on the nominal channel inlet velocity V_0.

Figure 10 shows the time history of both the open-loop and closed-loop response to a band-limited white noise disturbance. The controller reduces the amplitude of the deviation in longitudinal velocity from nominal at the performance variable z in about 50 seconds. Figure 11 shows the power spectral density plot of the open-loop and closed-loop responses to the band-limited white noise disturbance. A decrease of up to 70 dB in the closed-loop response is seen across the frequency range, up to about 5 Hz.

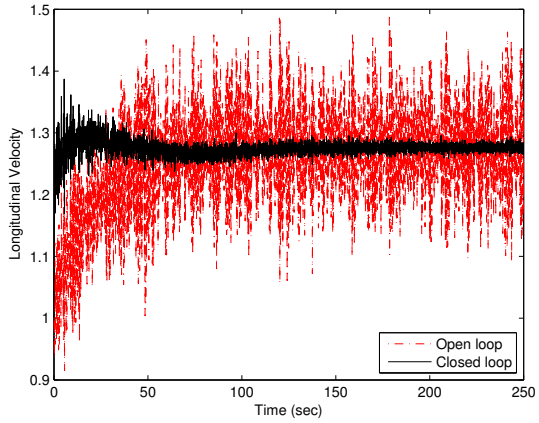

Fig. 10. Open-loop and closed-loop longitudinal performance velocity response for a band-limited white noise disturbance.

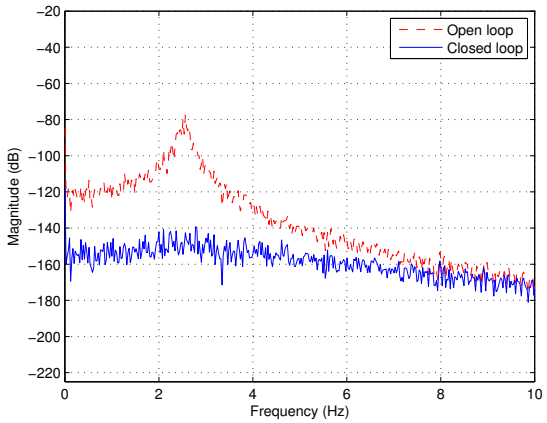

Fig. 11. Open-loop and closed-loop power spectrum for a band-limited white noise disturbance.

In addition to varying the controller order, the noise power of the band-limited white noise disturbance is increased. It is found that noise power greater than 0.0001 W/Hz excites nonlinear dynamics of the flow, which the controller is not able to suppress by a substantial amount.

VII. Conclusion

Adaptive flow control using the ARMARKOV disturbance rejection algorithm was demonstrated by means of a 2D channel Poiseuille flow CFD simulation. No first-principles model was derived or is needed for this adaptive disturbance rejection algorithm; instead, system identification was used to estimate the numerator coefficients of the transfer functions from the control inputs to the performance variable. Disturbance rejection was demonstrated for single-tone, dual-tone, and band-limited white noise disturbances. Disturbance rejection of up to 120 dB, between 0.01 Hz and 1 Hz, for both the single-tone and dual-tone cases was achieved, along

with up to 70 dB rejection, up to 5 Hz, in the band-limited white noise case. The combination of CFD simulation and the adaptive disturbance rejection algorithm thus constitutes a technique for controlling a fluid without analytical modeling and with limited empirical (identification) modeling.

REFERENCES

[1] T. R. Bewley, "Flow control: new challenges for a new renaissance," *Progress in Aerospace Sciences*, vol. 37, no. 1, pp. 21–58, 2001.

[2] O. M. Aamo and M. Krstić, *Flow Control by Feedback: Stabilization and Mixing*, 1st ed. Great Britain: Springer, 2003.

[3] S. S. Joshi, J. L. Speyer, and J. Kim, "A systems theory approach to the feedback stabilization of infinitesimal and finite-amplitude disturbances in plane Poiseuille flow," *J. of Fluid Mechanics*, vol. 332, pp. 157–184, 1997.

[4] ——, "Finite dimensional optimal control of Poiseuille flow," *J. Guid. Contr. Dynamics*, vol. 22, no. 2, pp. 340–348, 1999.

[5] L. Cortelezzi, K. Lee, J. Kim, and J. Speyer, "Skin-friction drag reduction via robust-order linear feeback control," *Int. J. Comput. Fluid Dyn.*, vol. 8, no. 1-2, pp. 79–92, 1998.

[6] L. Cortelezzi and J. Speyer, "Robust reduced-order controller of laminar boundary layer transitions," *Physical Review E*, vol. 58, no. 2, pp. 1906–1910, 1998.

[7] A. Emami-Naeini, S. A. McCabe, D. de Roover, J. L. Ebert, and R. L. Kosut, "Active control of flow over a backward-facing step," in *Proc. Conf. Dec. Contr.*, Seville, Spain, 2005, pp. 7366–7371.

[8] P. Christofides and A. Armaou, "Nonlinear control of Navier-Stokes equations," in *Proc. Amer. Cont. Conf.*, Philadelphia, PA, 1998, pp. 1355–1359.

[9] R. Vazquez and M. Krstić, "A closed-form feedback controller for stabilization of linearized Navier-Stokes equations: The 2D Poiseuille flow," in *Proc. Conf. Dec. Contr.*, Seville, Spain, 2005, pp. 7358–7365.

[10] J. A. Burns and J. Singler, "Feedback control of low dimensional models of transition to turbulence," in *Proc. Conf. Dec. Contr.*, Seville, Spain, 2005, pp. 3140–3145.

[11] T. R. Bewley, P. Moin, and R. Temam, "DNS-based predictive control of turbulence: an optimal benchmark for feedback algorithms," *Journal of Fluid Mechanics*, vol. 447, pp. 179–225, 2001.

[12] D. Greenblatt and I. Wygnanski, "Dynamic stall control by periodic excitation, Part 1: NACA 0015 parametric study," *Journal of Aircraft*, vol. 38, no. 3, pp. 430–438, 2001.

[13] D. Greenblatt, B. Nishri, A. Darabi, and I. Wygnanski, "Dynamic stall control by periodic excitation, Part 2: Mechanisms," *Journal of Aircraft*, vol. 38, no. 3, pp. 439–447, 2001.

[14] D. Greenblatt and I. J. Wygnanski, "The control of flow separation by periodic excitation," *Progress in Aerospace Sciences*, vol. 36, pp. 487–545, 2000.

[15] L. Henning, D. Kuzmin, V. Mehrmann, M. Schmidt, A. Sokolov, and S. Turek, "Flow control on the basis of a FEATFLOW-MATLAB coupling," in *Proc. Conf. Active Flow Contr.*, Berlin, Germany, 2006.

[16] K. Kim, M. Kerr, A. Beskok, and S. Jayasuriya, "Frequency-domain based feedback control of flow separation using synthetic jets," in *Proc. Amer. Contr. Conf.*, Minneapolis, MN, 2006, pp. 5318–5323.

[17] O. Lehmann, M. Luchtenburg, B. R. Noack, R. King, M. Morzynski, and G. Tadmor, "Wake stabilization using POD Galerkin models with interpolated modes," in *Proc. Conf. Dec. Contr.*, Seville, Spain, 2005, pp. 500–505.

[18] M. Luchtenburg, G. Tadmor, O. Lehmann, B. R. Noack, R. King, and M. Morzynski, "Tuned POD Galerkin models for transient feedback regulation of the cylinder wake," in *Proc. AIAA Aerospace Sciences Meeting and Exhibit*, Reno, NV, 2006, AIAA-2006-1407.

[19] L. Henning and R. King, "Multivariable closed-loop control of the reattachment length downstream of a backward-facing step," in *Proc. 16^{th} IFAC World Congress*, Prague, Czech Republic, 2005.

[20] L. Cattafesta, D. Shukla, S. Garg, and J. Ross, "Development of an adaptive weapons-bay suppression system," Bellevue, WA, 1999, AIAA-1999-1901.

[21] M. Kegerise, L. Cattafesta, and C. Ha, "Adaptive identification and control of flow-induced cavity oscillations," in *Proc. AIAA Flow Control Conf.*, St. Louis, MO, 2002, AIAA-2002-3158.

[22] R. King, R. Becker, M. Garwon, and L. Henning, "Robust and adaptive closed-loop control of separated shear flows," in *Proc. AIAA Flow Control Conf.*, Portland, OR, 2004, AIAA-2004-2519.

[23] R. King, R. Becker, G. Feuerbach, L. Henning, R. Petz, W. Nitsche, O. Lemke, and W. Neise, "Adaptive flow control using slope seeking," in *Proc. IEEE Mediterranean Conf. Contr. Automation*, Ancona, Italy, 2006.

[24] M. Garwon and R. King, "A multivariable adaptive control strategy to regulate the separated flow behind a backward-facing step," in *Proc. 16^{th} IFAC World Congress*, Prague, Czech Republic, 2005.

[25] L. Henning and R. King, "Drag reduction by closed-loop control of a separated flow over a bluff body with a blunt trailing edge," in *Proc. Conf. Dec. Contr.*, Seville, Spain, 2005, pp. 494–499.

[26] M. Rizzo, M. Santillo, A. Padthe, J. B. Hoagg, S. Akhtar, K. Powell, and D. S. Bernstein, "CFD-based adaptive flow control using ARMARKOV disturbance rejection," in *Proc. Amer. Contr. Conf.*, Minneapolis, MN, 2006, pp. 3783–3788.

[27] M. Santillo, J. B. Hoagg, D. S. Bernstein, and K. Powell, "CFD-based adaptive flow control for steady flow field modification," in *Proc. Conf. Dec. Contr.*, San Diego, CA, 2006, pp. 3105–3110.

[28] A. Pillarisetti and L. N. Cattafesta, "Adaptive identification of fluid-dynamic systems," in *Proc. AIAA Fluid Dynamics Conf.*, Anaheim, CA, 2001, AIAA 2001-2978.

[29] "CFD Flow Modeling Software," Fluent Inc., September 2006, http://www.fluent.com/.

[30] R. Venugopal and D. S. Bernstein, "Adaptive disturbance rejection using ARMARKOV/Toeplitz models," *IEEE Trans. Contr. Syst. Technol.*, vol. 8, no. 2, pp. 257–269, 2000.

[31] S. Akhtar and D. S. Bernstein, "Discrete-time adaptive stabilization and disturbance rejection for minimum phase plants," in *Proc. Conf. Dec. Contr.*, Seville, Spain, 2005, pp. 2236–2241.

[32] J. C. Akers and D. S. Bernstein, "ARMARKOV least-squares identification," in *Proc. Amer. Contr. Conf.*, Albuquerque, NM, 1997, pp. 186–190.

[33] ——, "Time-domain identification using ARMARKOV/Toeplitz models," in *Proc. Amer. Contr. Conf.*, Albuquerque, NM, 1997, pp. 191–195.

[34] S. Akhtar and D. S. Bernstein, "Optimal adaptive feedback disturbance rejection," in *Proc. ACTIVE 04*, Williamsburg, VA, 2004.

[35] J. Chandrasekar, L. Liu, D. Patt, P. P. Friedmann, and D. S. Bernstein, "Active noise cancellation for systems with uncertain dynamics using adaptive harmonic steady state control," in *Proc. ACTIVE 04*, Williamsburg, VA, 2004.

[36] J. B. Hoagg and D. S. Bernstein, "Discrete-time adaptive feedback disturbance rejection using a retrospective performance measure," in *Proc. ACTIVE 04*, Williamsburg, VA, 2004.

[37] J. B. Hoagg, S. L. Lacy, R. Venugopal, and D. S. Bernstein, "Adaptive control of a flexible membrane using acoustic excitation and optical sensing," in *AIAA Guid. Nav. Contr. Conf.*, Austin, TX, 2003, AIAA-2003-5430.

[38] S. L. Lacy, R. Venugopal, and D. S. Bernstein, "ARMARKOV adaptive control of self-excited oscillations of a ducted flame," in *Proc. Conf. Dec. Contr.*, Tampa, FL, 1998, pp. 4527–4528.

[39] H. Sane and D. S. Bernstein, "Active noise control using an acoustic servovalve," in *Proc. Amer. Contr. Conf.*, Philadelphia, PA, 1998, pp. 2621–2625.

[40] H. Sane, R. Venugopal, and D. S. Bernstein, "Disturbance rejection using self-tuning ARMARKOV adaptive control with simultaneous identification," *Trans. Contr. Sys. Tech.*, vol. 9, pp. 101–106, 2001.

[41] J. B. Hoagg, S. L. Lacy, and D. S. Bernstein, "Broadband adaptive disturbance rejection for a deployable optical telescope," in *Proc. Amer. Contr. Conf.*, Portland, OR, 2005, pp. 4953–4958.

[42] S. Akhtar and D. S. Bernstein, "Logarithmic Lyapunov functions for direct adaptive stabilization with normalized adaptive laws," *Int. J. Contr.*, vol. 77, pp. 630–638, 2004.

[43] G. Goodwin, P. Ramadage, and P. Caines, "Discrete-time multivariable adaptive control," *IEEE Transactions Automatic Control*, vol. 25, pp. 449–456, 1980.

[44] S. Akhtar and D. S. Bernstein, "Lyapunov-stable discrete-time model reference adaptive control," *Adaptive Contr. Signal Proc.*, vol. 19, pp. 745–767, 2005.

[45] J. B. Hoagg and D. S. Bernstein, "Adaptive stabilization, command following, and disturbance rejection for minimum phase discrete-time systems," in *Proc. Conf. Dec. Contr.*, San Diego, CA, 2006, pp. 471–476.

[46] J. Hong and D. S. Bernstein, "Bode integral constraints, colocation, and spillover in active noise and vibration control," *IEEE Trans. Contr. Syst. Technol.*, vol. 6, no. 1, pp. 111–120, 1998.